Regulated Emissions and Detailed Particle Characterisation for Diesel and RME Biodiesel Fuel Combustion with Varying EGR in a Heavy-Duty Engine

Novakovic, Maja; Shamun, Sam; Malmborg, Vilhelm; Kling, Kirsten I; Kling, Jens; Vogel, Ulla B; Tunestål, Per; Pagels, Joakim; Tunér, Martin

Published in:
SAE Technical Paper Series

DOI:
10.4271/2019-01-2291

2019

Document Version:
Peer reviewed version (aka post-print)

JSAE 20199246
SAE 2019-YY-YYYY

Regulated Emissions and Detailed Particle Characterisation for Diesel and RME Biodiesel Fuel Combustion with Varying EGR in a Heavy-Duty Engine

Maja Novakovic[a], Sam Shamun[a], Vilhelm B. Malmborg[b], Kirsten I. Kling[c], Jens Kling[c], Ulla B. Vogel[d], Per Tunestal[a], Joakim Pagels[b], Martin Tuner[a]

[a]Division of Combustion Engines, Lund University, Box 118, 22100 Lund, Sweden
[b]Division of Ergonomics and Aerosol Technology, Lund University, Box 118, 22100 Lund, Sweden
[c]DTU Nanolab, Fysikvej 307, 2800 Kgs. Lyngby, Denmark
[d]National Research Centre for the Working Environment, Lerso Parkalle 105, 2100 Copenhagen, Denmark

ABSTRACT

This study investigates particulate matter (PM) and regulated emissions from renewable rapeseed oil methyl ester (RME) biodiesel in pure and blended forms and contrasts that to conventional diesel fuel. Environmental and health concerns are the major motivation for combustion engines research, especially finding sustainable alternatives to fossil fuels and reducing diesel PM emissions. Fatty acid methyl esters (FAME), including RME, are renewable fuels commonly used from low level blends with diesel to full substitution. They strongly reduce the net carbon dioxide emissions. It is largely unknown how the emissions and characteristics of PM get altered by the combined effect of adding biodiesel to diesel and implementing modern engine concepts that reduce nitrogen oxides (NOx) emissions by exhaust gas recirculation (EGR). Therefore, the exhaust from a single-cylinder Scania D13 heavy-duty (HD) diesel engine fuelled with petroleum-based MK1 diesel, RME, and a 20% RME blend (B20), was sampled while the inlet oxygen concentration was stepped from ambient to very low by varying EGR. Regulated gaseous emissions, mass of total black carbon (BC) and organic aerosol (OA), particle size distributions and the soot nanostructure by means of transmission electron microscopy (TEM), were studied. For all EGR levels, RME showed reduced BC emissions (factor 2 for low and 3-4 for higher EGR) and total particulate number count (TPNC) compared with diesel and B20. B20 was closer to diesel than RME in emission levels. RME opens a significant possibility to utilise higher levels of EGR and stay in the region of low NOx, while not producing more soot than with diesel and B20. Adding EGR to 15% inlet O_2 did not affect the nanostructure of PM. A difference between the fuels was noticeable: branched agglomerates of diesel and RME were composed of many primary particles, whereas those of B20 were more often “melted” together (necking).

INTRODUCTION

Major stimulation for research within the area of internal combustion engines (ICEs) are environmental and health concerns. Finding sustainable substitutes for fossil fuels and reducing particulate matter (PM) in diesel exhaust are of particular interest.

Carbon dioxide is a long-lived greenhouse gas (GHG) that is the dominant contributor to climate emissions worldwide, being responsible for 55-60% of anthropogenic radiative forcing [1]. Transportation sector is responsible for approximately 16% of global net CO_2 emissions [2][3]. CO_2 emissions from the transport sector in the United States of America [4] and in the European Union [5] were accountable for more than 25% of their total CO_2 emissions in year 2016. Black carbon (BC), a component of PM, and also referred to as soot, is a short-lived climate pollutant, and the second largest contributor to climate change after CO_2 [6].

BC is a product of incomplete combustion of hydrocarbon-based fuels, i.e. both of combustion of fossil fuels and renewable fuels. BC adds strongly to the radiative forcing, warming the climate globally; it has a strong regional influence and is responsible for a significant proportion of the local forcing to date [6]. BC significantly contributes to changes in global surface temperature and the vertical structure of temperature in the atmosphere [7][8]. Studies have also documented the impact of BC deposited on the cryosphere, leading to enhanced melting rates of snow, ice and frozen ground [8].

Regarding PM chemical composition, many studies focus on organic aerosols (OAs) because they contribute with 20-90% to the total submicron particles mass [9][10]. OA is dynamic and continually evolves in the atmosphere, which strongly influences the effects of PM on climate and air quality. OA can be either

directly emitted by different sources, including anthropogenic (traffic and combustion activities), or produced via secondary formation after the oxidation of volatile organic compounds (VOCs) [11][12]. Therefore, reliable source identification and quantification of OAs is needed to accurately predict regional and global OA distributions and properties and thus the associated health and climate effects [9].

The compression ignition (CI) diesel engine has been developing and the levels of harmful emissions in the exhaust gases have been reduced as a consequence. At the same time, the efficiency of the engine and the systems around it have improved. Still, these advances are not enough to overcome all challenges. Diesel exhaust particles (DEPs) vary in their size, composition, solubility and therefore also in their toxic properties. Ambient aerosol particles (including DEPs) easily enter human pulmonary system. Ultrafine particles (UFPs) smaller than 100 nm are deposited in the alveolar region of lungs that have only weak nanoparticle elimination mechanisms. UFPs may translocate beyond the lung and cause adverse effects on the central nervous system, extrapulmonary organs and cause dysfunction of blood vessels causing negative cardiac effects [13][14].

Prices of crude oil, as well as demand for the transportation fuel, continue to rise. The supply of the fossil fuels is limited and the reserves will be depleted eventually, resulting in an urgent need for substitutes to the conventional ICE fuelled by petroleum-based diesel or gasoline. The alternative renewable and sustainable fuels are seen as feasible solutions with which the net CO_2 emissions of the transportation sector can be reduced substantially. However, less is known on changes in PM emissions, their properties and eventually their effects of relevance for air quality changes when introducing novel biofuels.

The tightening of the legislated particulate emission limits drives further development of the diesel engines and fuels compatible with them. Since year 2011 (Euro 5b), the European emissions regulation includes measurement of solid [1] particle number (SPN) > 23 nm for approval of diesel light-duty engines, in addition to the previously regulated levels of allowed PM mass emissions [15]. The current SPN limit for on-road heavy-duty (HD) CI engines was introduced in 2013 (Euro VI) [16]. Particles of size below 23 nm are currently not included in these emission regulations, but their monitoring is highly recommended [17].

Understanding the properties of raw engine emissions also contributes to the development and optimisation of exhaust aftertreatment technologies, such as diesel oxidation catalysts (DOC), diesel particulate filters (DPF) and selective catalytic reduction (SCR), which in their turn can alter the physical and chemical composition of PM. Nanostructure of soot is especially important for the oxidation kinetics in the exhaust aftertreatment [18][19].

Fatty acid methyl ester (FAME) fuels, commonly called biodiesel, can be produced from primary vegetable oils such as soy oil, palm oil, coconut oil, sunflower oil etc. Rapeseed oil methyl ester (RME) is produced by esterification of rapeseed oil by use of biomethanol. In Europe, most vehicles with CI engines currently use low level blends of FAME in diesel. The blending of increasing fractions of oxygen containing FAME biodiesel fuels produced from renewable biomass resources into fossil diesel is currently encouraged to mitigate CO_2 emissions [20]. The use of pure biodiesel would also be another effective way for fossil CO_2 emission reduction, which is possible in modern diesel engines without changes to the fuel injection system [21].

Reduced BC and increased OA emissions were previously reported for both low and high level blends of FAME in diesel [22]. These studies concerned cases with no or low exhaust gas recirculation (EGR) levels. Higher EGR levels for medium-duty engines indicated higher PM reduction rates [23]. Similar trends were seen for measured smoke values in HD engines [24]. In addition, a decrease in the BC primary and aggregate particle sizes, increases in the fractal dimension of the agglomerates and a greater disorder of the soot nanostructure were also observed when using FAME biodiesels [25].

Engine out NOx emissions have consistently been found slightly higher with biodiesel fuel blends compared to petroleum-based diesel. This is proposed to be due to the double bonds present in biodiesel leading to slightly higher adiabatic flame temperatures [26], and also due to the lowered in-cylinder soot levels, thus lower radiation heat transfer, resulting again in higher in-cylinder temperatures [27].

The addition of biodiesel to diesel alters PM and other emissions. Modern engine concepts that reduce NOx emissions by using EGR up to high levels additionally influence particle properties. The combined effects of biodiesel blends and modern engine concepts on the particle characteristics are mainly unknown.

The objective of this paper is twofold:

1. to experimentally investigate and characterise particulate mass of BC and total OA, particle number weighted size distributions, chemical composition and micro- and nanostructure of the particles emitted from combustion of RME biodiesel, a petroleum-based diesel fuel and their blend in a modern HD CI engine operating at stationary engine conditions while intake air oxygen concentration is decreased from 20.95% to ~8% by increasing EGR;

2. to study the effects of the fuel composition and engine operation conditions on the regulated exhaust gases.

[1] In particle measurement program (PMP) protocol from EU, solid particles refer to those particles that survive heating to 300°C in the measurement set-up prior to particle counting.

METHOD

ENGINE SETUP AND FUELS

The experiments were performed in a Scania D13 HD six-cylinder diesel engine modified in such a way that only one cylinder was operating while the other five were motored without compression. The specifications of the experimental engine are given in Table 1 and its schematic diagram in Figure 1.

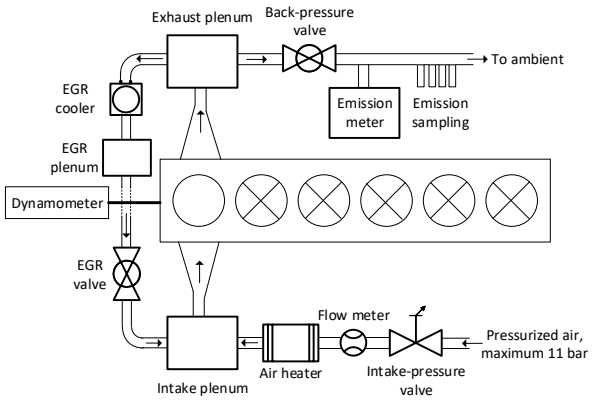

Figure 1. Schematic diagram of the experimental engine, adapted from [28].

The engine was supercharged with an external compressor providing pressurised air with a 7.5 kW heater located between the fresh air supply and intake manifold. The engine test rig was equipped with an adjustable EGR system which consisted of an EGR valve and an exhaust backpressure valve. The cooled, high-pressure EGR was introduced to the intake plenum for blending with pressurised fresh air. The existing equipment was used and therefore the engine piston was of the standard production shape and the engine was equipped with XPI common rail injection system with an injector with 10 holes and 148° spray angle. Four sampling probes for the emission analysers were placed in the middle the exhaust pipe at a distance specified by the manufacturers of the measurement equipment in order to avoid flow disturbances. Measurements were conducted on raw engine-out exhaust without using aftertreatment systems.

Table 1. Single cylinder engine specifications.

Displaced volume	1966 cm^3
Stroke	160 mm
Bore	130 mm
Connecting rod length	255 mm
Compression ratio	17.3:1
Number of valves	4
Swirl ratio	2.1
Inlet valve close	-141 CAD ATDC
Inlet valve open	2° BTDC @ 0.15 mm lift

Two different fuels and their mixture were used in this study: petroleum-based Swedish MK-1 diesel (also marked as B0), pure RME biodiesel made for low level blends in Nordic climate (B100) and their mixture of 20 volume-% RME and 80 volume-% MK-1 (B20), the specifications of which are listed in Table 2. See Table A-2 in Appendix A for the detailed chemical composition of RME and Table A-1 for the nomenclature of the three fuels. There were not any additives added to fuels before the experiments. The lubrication oil in the engine was Statoil PowerWay GE40, a lubricant with low ash content used mainly for engines operated on biogas.

In order to understand possible origin of the PM in the emissions, the metal traces in the engine lubricant sampled before and after the experiments, as well as in the fuels, were analysed. The H/C and O/C values in Table 2 are calculated from the elemental analysis of the fuels and fuel specifications (see Table A-2).

Table 2. Fuel specifications.

	RME	MK-1 diesel
CN	52	53-57
H/C	1.896	2
O/C	0.103	0.002
Q_{LHV}	38 MJ/kg	43.2 MJ/kg
$(A/F)_S$	12.37	14.5

EMISSION MEASUREMENT SYSTEMS

An assortment of advanced emission measurement equipment was used in this study in order to create a more comprehensive image of the PM and gaseous emissions.

Exhaust gas analyser

The engine-out gaseous emissions were measured by a commercial AVL AMA i60 system. The CO_2 concentration was measured both in the intake manifold and in the exhaust to provide the data for the calculation of the EGR level. The dry CO and CO_2 were measured with an infrared detector (IRD), whereas the wet NO and NO_x ($NO+NO_2$) were measured using a chemiluminescence detector (CLD). The wet total hydrocarbons (THC) was measured by a flame ionisation detector (FID). The CH_4 concentration is measured within the THC.

The EGR level used in this study was calculated as a ratio between measured concentrations of carbon dioxide in the intake and carbon dioxide in the exhaust, expressed as percentage, as shown in Eq. (1).

$$EGR = \frac{CO_{2_{Inlet}}}{CO_{2_{Exhaust}}} \cdot 100\% \quad (1)$$

The O_2 concentration in the exhaust was measured by a paramagnetic detector (PMD), and the intake O_2 concentration was calculated according to the Eq. (2).

$$O_{2_{Inlet}} = EGR \cdot \left(O_{2_{Exhaust}} - O_{2_{Ambient}}\right) + O_{2_{Ambient}} \quad (2)$$

(where $O_{2_{Exhaust}}$ is the oxygen concentration measured in the exhaust, and $O_{2_{Ambient}}$ is the ambient oxygen concentration set to a constant value of 20.95%).

Particulate matter

PM from diesel combustion is a complex mixture of particles with different sizes and composition. In this study, the focus was laid on chemical composition (BC and OA emissions), the particle size distribution and nanostructure of emitted soot.

The exhaust gas was sampled from the middle of the exhaust pipe at the angle of 90°, and led to the dilution setup presented in Figure 2. The first stage dilution (Dekati ejector) used a dilution factor of 15. It was done with hot air at 150 °C for all operation points with B20 due to water condensation. At other operation points, cold dilution was used. The gas was then led through a 200 ml unheated residence tube and then diluted additional 4 times with cold air in the second stage Dekati diluter 2.

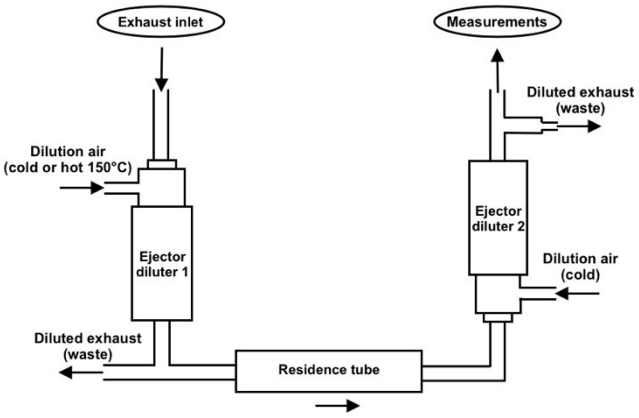

Figure 2. Schematic diagram of the dilution setup.

An AVL micro-soot sensor (MSS) was used to continuously measure the equivalent black carbon (eBC) mass concentration of soot in the engine-out exhaust stream [29]. Measurements are based on the photo-acoustic principle. Inside of the measurement cell, an amplitude modulated 808 nm light beam is absorbed by airborne particles. This makes the carrier gas expand and contract due to periodic heating and cooling, and in that way produce periodic pressure waves. The pressure waves are a measure of the particle absorptive properties (at 808 nm), and are gathered by sensitive microphones and translated into a soot mass concentration (eBC) by assuming a conversion factor from absorption to mass concentration. The BC part of the PM absorbs, while OA is essentially transparent at this wavelength, thus not seen. The MSS is able to measure with a sensitivity of 1 µg/m^3 in the range from 0.001 to 1000 mg/m^3.

The differential mobility spectrometer (DMS) Cambustion DMS500 was used to determine the particle size distribution (5 nm - 1000 nm) [30]. Measurements were sampled with a frequency of 1 Hz. At the sampling probe, a cyclone was used to dilute the exhaust gas at a ratio of 5:1. After dilution, the particles are charged by a unipolar corona charger. According to the charge they receive, which is proportional to their surface area and their size, they are separated according to electrical mobility while passing a strong radial electrical field. Particles with lower electrical mobility (larger size) travel further along the column. This principle is also known as electrical mobility classification. After the particles get deposited on one of the 22 electrometer detectors, the measured electrical current signals are finally transferred into a number particle size distribution using the built-in diesel soot inversion matrix.

The total OA was analysed using a soot-particle aerosol mass spectrometer (SP-AMS) [31]. The SP-AMS was run in single or dual vaporiser mode. In the single vaporiser mode, particles are flash vaporised upon impaction on a heated (600 °C) tungsten surface. In the dual vaporiser mode, refractory black carbon (rBC) containing particles is vaporised using an intracavity Nd:YAG laser (1064 nm). The vapours are then ionised (70 eV electron ionisation) and detected in a HR-ToF mass spectrometer. Total OA concentrations were derived from the dual vaporiser mode. The total OA signal intensity depends on the vaporisation mode. To derive OA mass concentrations, the dual vaporiser total OA signals were multiplied by a correction factor of 0.5 which was obtained from the linear regression analysis of a large number of total OA single mode and dual vaporiser mode ratios (R^2=0.93).

Aerosol samples were collected using an electrostatic precipitator (nanometre aerosol sampler model 3089 TSI) onto thin lacy carbon coated copper grids (Cu-400LD, Pacific Grid-Tech). The transmission electron microscopy (TEM) grids were analysed in a transmission electron microscope FEI Tecnai T20 G2. High-resolution images were recorded with DigitalMicrograph software [32] using a Gatan US1000 bottom mounted camera. Following the procedures used in previous work [33], a series of high-resolution images was recorded for every sample.

Images clearly displaying the configuration of graphene layers in soot particles were chosen for further analysis. This bright and dark contrast of parallel segments differs significantly from the homogenous, amorphous contrast of an underlying amorphous carbon film. The distance between the parallel layers was measured by a profile tool (dark to dark or bright to bright). For each sample, approximately 100 values were determined. The accuracy lies within ± 0.027 nm at a resolution of 38 pixel/nm. Tortuosity was measured manually as described in [34] and [35] as the ratio of the lamella length to the distance between its two end points (see also Figure 10a in [35]). Fringe length and tortuosity as well as primary particle diameter were determined with ImageJ software [36]. For particle diameter, a spherical particle was assumed and the diameter of this sphere measured.

ENGINE OPERATION CONDITIONS AND EXPERIMENT STRATEGIES

The parameter that was varied throughout the experiment was the intake O_2 concentration, i.e. the EGR level. The EGR gas was cooled before being introduced to the intake manifold and mixed with ambient temperature air. Six levels of O_2 were studied for diesel and RME fuels and five levels for B20 within the intake O_2 span starting at the ambient concentration at 20.95% (without any EGR) and reaching the very low levels of ~8% O_2 (close to 60% EGR).

The four inlet oxygen concentrations which are comparable among the three fuels are:

1. 11.7% for RME and 11.4% for diesel,
2. 13.6% for RME and 13.3% for B20 and diesel,
3. 14.9% for RME, 15.4% for B20 and 15.2% for diesel,
4. 20.95% for all three fuels.

For improved readability, they will be marked throughout the Results and Discussion section as ~11.5%, ~13.5%, ~15% and ~21%, respectively.

The data used in this study were collected from the engine and averaged from 300 engine cycles measured under steady state engine operation conditions at the constant rotational speed of 1200 rpm. Gross indicated mean effective pressure ($IMEP_G$) at the starting point with the ambient air O_2 concentration at the intake (20.95%) was 6 bar, and the energy content of the injected fuel was kept constant. The combustion phasing was also kept constant throughout the experiment with CA50 at ~5 crank angle degrees after top dead centre (CAD ATDC) by adjusting start of injection (SOI) timing of a single fuel injection at 1200 bar common rail pressure. The intake mixture was at constant temperature of 100 °C. The observed lambda (λ) values are based on the measured emissions data. λ was the same for all three fuels λ≈2.0 at the starting point at 20.95% intake O_2 concentration, then it decreased with decrease of the intake O_2 concentration, see Figure 3. At close to 10.5% intake O_2 the stoichiometric λ value is reached for diesel and B20, whereas RME reaches stoichiometry at close to 9.5% intake O_2.

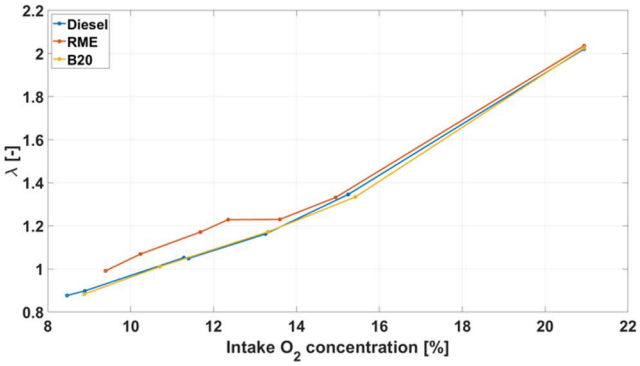

Figure 3. Lambda for different intake O_2 concentration for the three fuels. For fuels nomenclature see Table A-1 in Appendix A.

RESULTS AND DISCUSSION

GASEOUS EMISSIONS

Due to incomplete combustion, levels of indicated specific THC and CO emissions are rapidly increasing with the decrease in the oxygen available for the combustion below 13% and 15% for all three fuels, as shown in Figure 4 and Figure 5, respectively. The values of these emissions are almost at the same low levels for higher intake O_2 concentrations for all fuels, whereas RME has favourable emissions compared to diesel and B20 for lower intake oxygen. The horizontal green lines in Figure 4, Figure 5 and Figure 6 indicate the emission limits given by the current regulated emission standard Euro VI (THC: 0.13 g/kWh, CO: 1.5 g/kWh, and NOx: 0.4 g/kWh) [16].

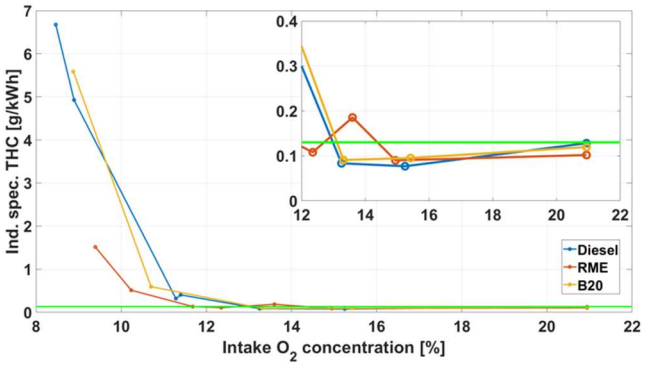

Figure 4. Indicated specific THC emissions for different intake O_2 concentration for the three fuels. For fuels nomenclature see Table A-1 in Appendix A.

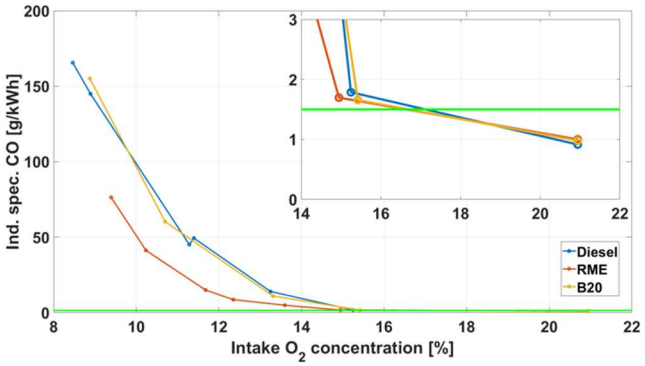

Figure 5. Indicated specific CO emissions for different intake O_2 concentration for the three fuels. For fuels nomenclature see Table A-1 in Appendix A.

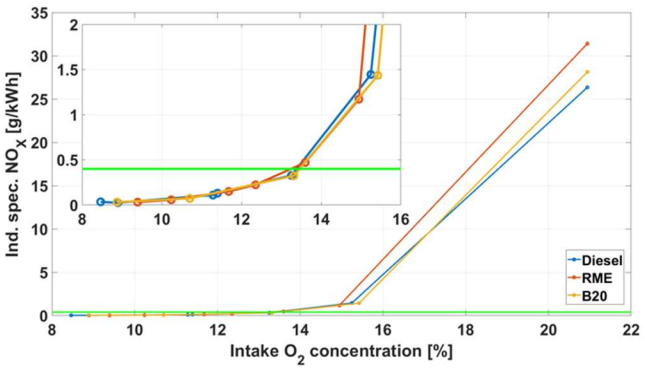

Figure 6. Indicated specific NOx emissions for different intake O_2 concentration for the three fuels. For fuels nomenclature see Table A-1 in Appendix A.

Indicated specific NOx emissions shown in Figure 6 follow a similar trend and stay under the regulated

limit for all three fuels in the region of low intake O_2 concentration. They increase drastically from around 15% and higher O_2 concentrations. The engine operation conditions were not in any way optimised to suppress any of the emissions in particular, but to compare how different EGR strategies influence regulated and unregulated emissions. This resulted in very high specific NOx emissions for the operation point without EGR where RME has the highest indicated specific NOx concentration followed by B20 and diesel (20% lower than RME). This is thought to be due to the additional oxygen available and the high degree of unsaturation of fatty acids in RME fuel (see Table A-1), as discussed in literature [37][38]. The fuel analysis of RME showed 10.6% mass oxygen content compared to that of diesel at 0.2%. With intake oxygen concentration of ~21%, RME was burning at a higher combustion temperature than diesel, causing higher NOx formation (Figure 7). Rate of heat release (RoHR) and in-cylinder pressure within a window of crank angles are also shown in Figure 7.

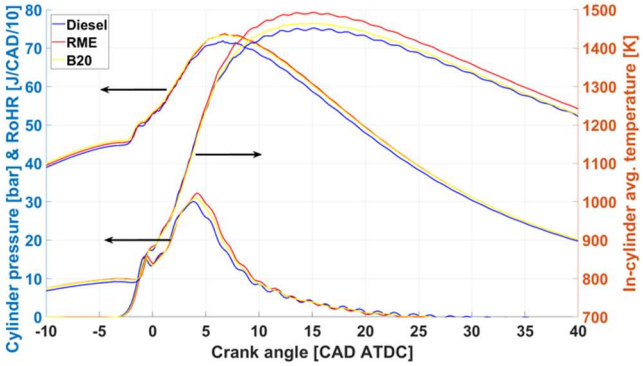

Figure 7. Heat release rate, in-cylinder pressure and average in-cylinder temperature at ~21% intake O_2 concentration for the three fuels. For fuels nomenclature see Table A-1 in Appendix A.

SOOT MASS CONCENTRATION

Figure 8 plots the soot (eBC) mass concentration measured by the AVL MSS as a function of the intake oxygen concentration for the three fuels over the range of intake O_2 levels.

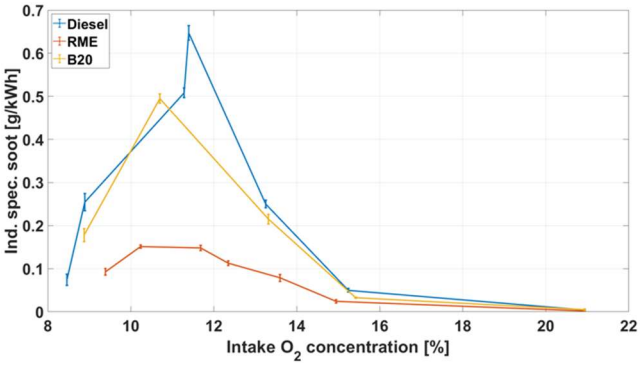

Figure 8. Indicated specific soot (eBC) mass concentration for different intake O_2 concentration for the three fuels. For fuels nomenclature see Table A-1 in Appendix A.

Soot emissions are strongly affected by EGR. The improvement in the soot levels is already seen for B20 compared to diesel, but RME emits considerably lower levels of soot over the whole range of intake O_2 concentration. It is reported in [22] that with low or no EGR FAME fuels decrease BC emissions by about a factor of 2, which matches our results at intake O_2 of ~21% and ~15%. The reduction factor increases to 3-4 at high EGR levels. This gives the possibility to utilise higher levels of EGR (lower intake O_2 concentration in Figure 8) with RME if the combustion is to result in the same soot levels like those produced when combusting diesel, and in that way stay in the region of low NOx, as well as CO and THC emissions.

Intake oxygen levels of ~15% that correspond to EGR of ~37-39%, are close to typical levels used in a modern HD CI engine. NOx values at intake O_2 of ~13.5% (~44% EGR) for all three fuels are only 23% to 40% of the NOx values at ~15% O_2. Indicated specific soot value of RME at intake O_2 of ~13.5% is below 0.1 g/kWh.

Lower soot levels for RME at the same operation conditions compared to diesel is an advantage in itself. These results are in accordance with the general conclusions in the available literature [39].

ORGANIC AEROSOL

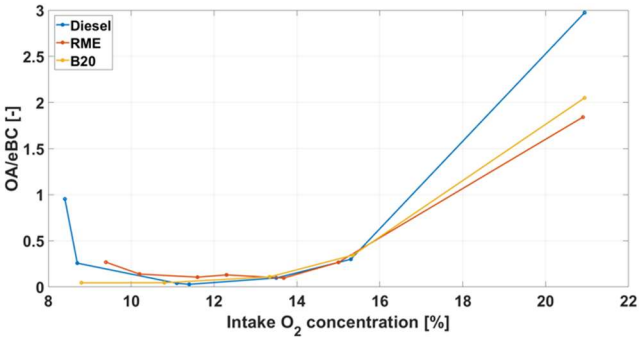

Figure 9. OA/eBC for different intake O_2 concentration for the three fuels. For fuels nomenclature see Table A-1 in Appendix A.

Figure 9 shows the ratio of (particle phase) OA measured with SP-AMS and eBC measured with MSS for different intake O_2 concentrations for the three fuels. At ~21% O_2 intake concentration, the organic part of the PM emissions is dominant, being three times higher than the eBC mass fraction for diesel and two times higher for B20 and RME. Since the combustion temperature of diesel at ~21% intake oxygen concentration is lower than that of RME, as shown in Figure 7, this difference between RME and diesel might be due to the incomplete combustion of lubrication oil that is consequently emitted in the exhaust. Previous studies report that the mass spectra of diesel aerosol components are dominated by lubrication oil spectral structures [40][41]. All three fuels have very low OA to eBC ratio for higher EGR levels. For oxygen concentrations lower than ~13.5% the ratio for RME is slightly higher than for B20 and diesel due to the lower soot emissions in that area. Finally, at the highest EGR level with 8.5% O_2 intake concentration, the ratio for diesel again rises and reaches the value of one. At this point a low amount of eBC is emitted, so the ratio of one shows low OA emissions. Additionally, the combustion efficiency is

very bad there as the engine is below stoichiometric conditions and emits unburned fuel.

PARTICLE NUMBER WEIGHTED SIZE DISTRIBUTION

Figure 10 presents the electrical mobility particle size distributions for the different intake oxygen concentrations for the three fuels, note the different scale for the particle number concentration for RME.

With no EGR, a nucleation mode dominated the emissions (20-30 nm), while for the remaining cases an accumulation mode at larger particle sizes dominated the number emissions (Figure 10). The particle count median diameter (CMD), geometrical standard deviation (GSD) and total particle number concentration (TPNC) for both nucleation mode particles and accumulation mode particles emitted with each of the three fuels measured by DMS are presented in Table B-1 in Appendix B. GSD describes the width of the size distribution centred around CMD [42]. The GSD values in Table B-1 for the accumulation mode (1.4-1.8) are similar or slightly lower than typical numbers for BC dominated aerosols generated primarily by coagulation. The GSDs of the nucleation mode (1.1-1.6) are lower as expected for aerosols generated primarily by condensation processes. CMD is equal to the diameter with highest concentration if the distribution is lognormal. CMDs of accumulation modes are, apart from being listed in Table B-1, also visually presented in Figure 11. Diesel has highest CMD values within the whole intake O_2 span (apart from the lowest O_2 level), followed by B20 and by RME, which is in agreement with the results available in literature, e.g. [43]. At the intake O_2 of ~21%, the values of accumulation CMD lie within the range of 44 nm to 55 nm, whereas the mean diameter increases for the lower O_2 values up to 125-160 nm.

Figure 12 shows the indicated specific TPNC for nucleation and accumulation modes, as well as the total values, depending on the intake O_2 concentration. Since the nucleation mode is pronounced only when operating without EGR, the indicated specific total TPNC trends follow the soot mass concentration measurements, see Figure 8, in the whole intake O_2 range apart from the starting point at ~21%. Nucleation mode in Figure 12 contains particles of size 5 nm and above, whereas emissions legislations regulate only particles larger than 23 nm.

There are four operation points at which the intake oxygen levels are comparable among the three fuels (~11.5%, ~13.5%, ~15%, ~21%). Firstly, total TPNC of RME is lower than half the value for diesel at intake O_2 concentration of ~11.5%. Secondly, at the intake O_2 concentration of ~13.5% total TPNC of RME is significantly lower, in particular it is only 6% of total TPNC of B20 and 5% of that of diesel. Thirdly, at the intake O_2 concentration of ~15% the advantage of RME is not as pronounced as in the previous point, since total TPNC of RME is similar to the one of B20 but more than three times lower than that of diesel. Finally, when EGR was not utilised RME and B20 had similar total TPNC, while that of diesel was 50% higher. Figure 12. clearly shows the advantage of using RME with EGR rates as high as 44% in terms of indicated specific TPNC under the studied engine operating conditions.

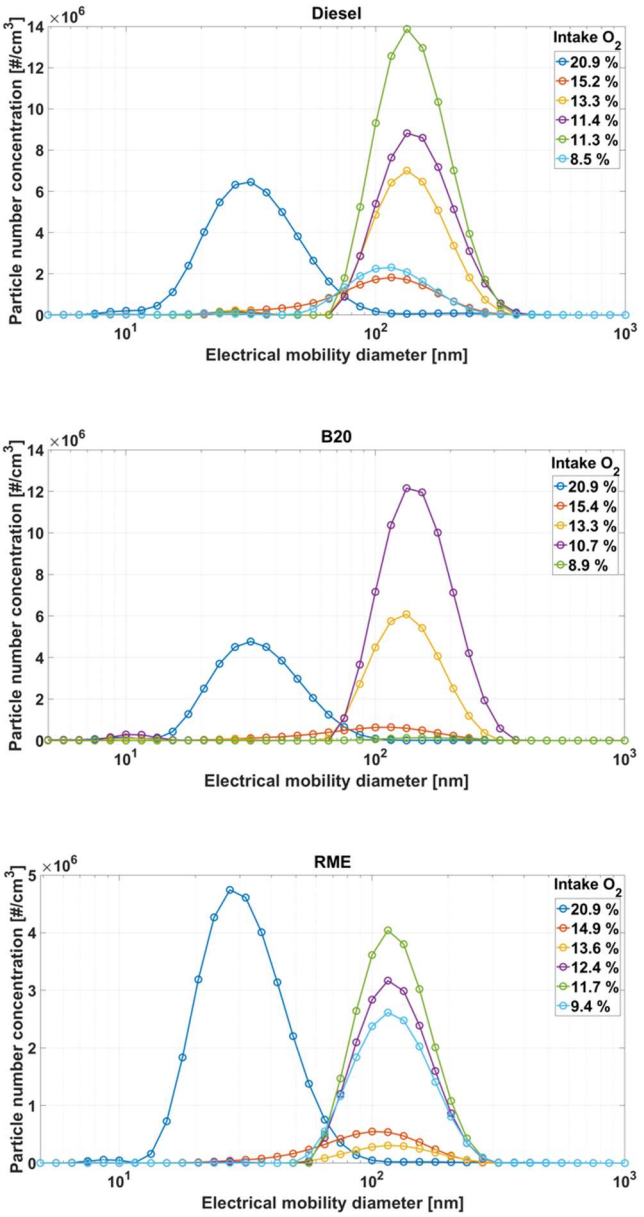

Figure 10. Number weighted particle size distributions for different intake O_2 concentration for the three fuels, top: diesel, middle: B20, and bottom: RME. For fuels nomenclature see Table A-1 in Appendix A.

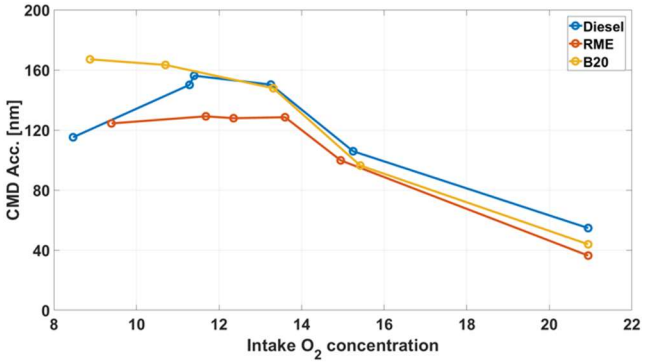

Figure 11. CMD of accumulation mode for different intake O_2 concentration for the three fuels. For fuels nomenclature see Table A-1 in Appendix A.

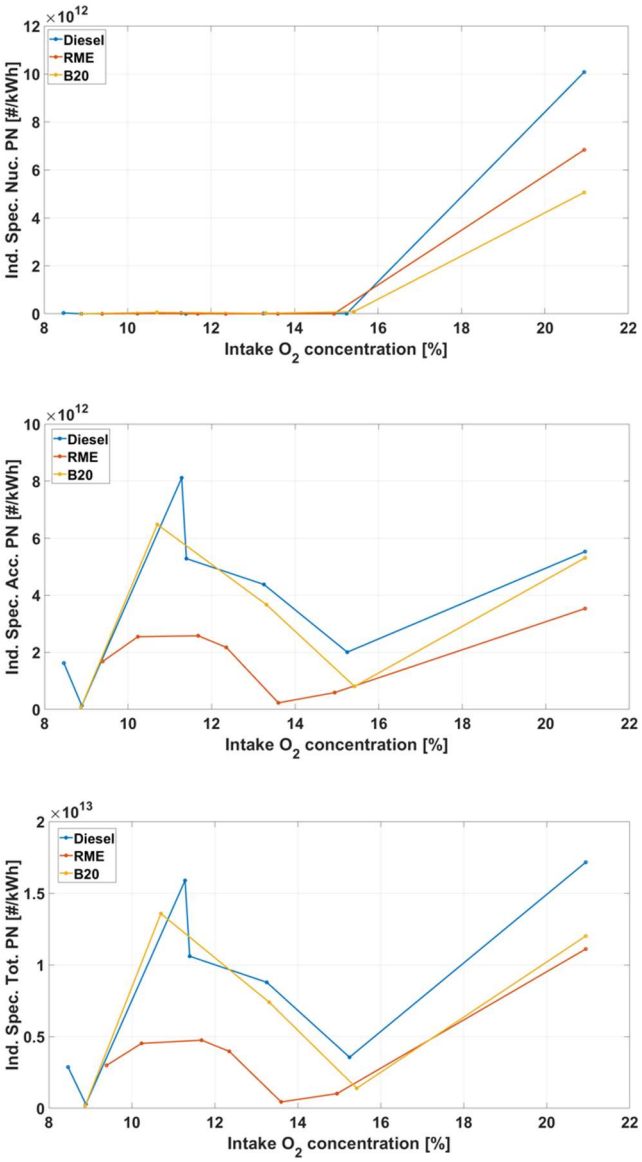

Figure 12. Indicated specific total particle number concentration for different intake O_2 concentration for the three fuels, top: nucleation mode, middle: accumulation mode, and bottom: total. For fuels nomenclature see Table A-1 in Appendix A.

TEM IMAGING

Quasi-graphitic layers or graphite-like structures were looked at when soot nanostructure was analysed. Graphite is the perfectly ordered version of carbon and has a lattice distance (the linear distance traversed by the atomic carbon layer planes) of 0.35 nm and a tortuosity (a measure of the curvature of the layer planes expressed as the ratio of fringe absolute length to straight-line distance between the visual endpoints of the fringe) of exact 1. The measures are taken from a two-dimensional projection of a three-dimensional, round-shaped structure. Adjacent fringes thus represent small graphitic blocks that build up a ball-shaped primary soot particle [44][45]. Soot aerosol is built up of agglomerates of primary soot particles. All these parameters, primary particle diameter, lattice distance, fringe length (i.e. lamella length) and tortuosity, can be used for inter-comparison and give an indication of the combustion conditions and physical-chemical properties of the aerosol [46][47].

Primary particle size, agglomerate size, appearance, lamella length and tortuosity were estimated and measured from images of samples collected by electrostatic precipitation directly onto TEM grids at engine intake O_2 concentration of ~15% and ~21% for RME, B20 and diesel. Measurements were performed on different positions distributed over the samples surface, to account for a representative distribution and a homogeneous sample was assumed. Overview images and high resolution images of soot particles can be seen in Appendix C in Figure C-1 for RME, Figure C-2 for B20 and Figure C-3 for diesel.

The overall appearance of the agglomerate form, shape and density does not show any obvious differences for each of the fuels at different inlet oxygen concentrations. The analysed lattice distances even within a single particle vary too much as to draw any inter-sample comparison conclusions. 20-25 agglomerates were analysed per sample. The difference between the different types of fuel is more pronounced.

Diesel and RME samples show branched agglomerates composed of several tens to hundreds of primary particles between 20 nm and 30 nm in diameter and lattice distances between 0.35 nm and 0.4 nm. In addition to the regular soot particles, diesel samples contain some fly ashes. Fly ashes are usually seen as perfectly round-shaped spheres, slightly bigger than the single soot particles, sometimes even up to a micron in size. They are thought to originate from the burned engine lubrication oil droplets, as explained in [48].

The samples collected from B20 also contain agglomerates of similar shape and size. The primary particles, however, seem to be “melted” together and individual particles are not possible to distinguish (necking). The structure is close to amorphous and only a few particles show a graphitic structure. Consequently, the few measured fringes appear shorter.

Figure 13 shows lamella lengths for all three fuels at two operation points each: at ~21% and ~15% intake O_2 concentrations, whereas tortuosity of these particles can be seen in Figure 14. The red central marks in the boxplot in Figure 13 and Figure 14 indicate the median lamella length and the median tortuosity, respectively. The bottom edges of the boxes show the 25th percentiles and top edges the 75th percentiles. The whiskers extend to the most extreme data points which are not considered outliers, and the outliers are plotted individually using the red + symbols. Fringes of RME particles are shorter at ~15% intake O_2 than at ~21%, which might indicate higher soot reactivity. On the contrary, tortuosity of RME soot particles at ~15% intake O_2 is slightly lower than at ~21%, which possibly leads to lower accessibility for oxidation. The difference between lamella lengths of analysed B20 soot particles at ~15% and ~21% intake O_2 is not statistically significant, and neither is the difference between their tortuosities at these two conditions. Diesel soot fringes are not statistically different at the two inlet oxygen levels. Diesel soot has

higher tortuosity at ~15% intake O_2 than at ~21%. Therefore, these results are not conclusive.

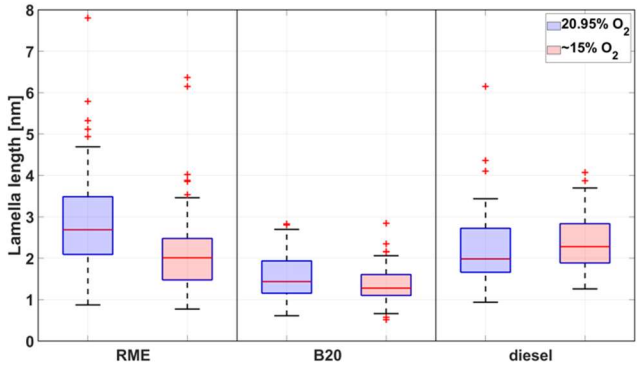

Figure 13. Lamella length for two intake O_2 concentration levels for the three fuels. Fuels nomenclature given in Table A-1 in Appendix A.

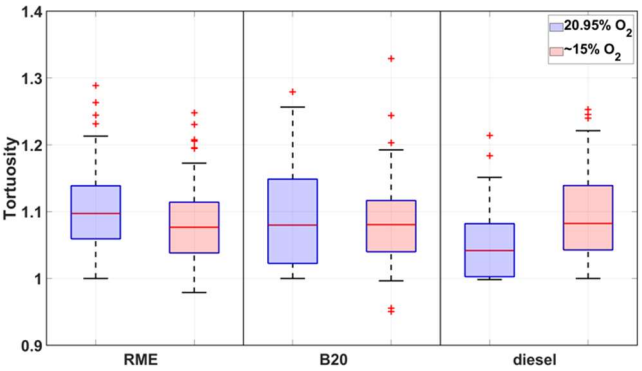

Figure 14. Tortuosity for two intake O_2 concentration levels for the three fuels. Fuels nomenclature given in Table A-1 in Appendix A.

FUEL AND ENGINE LUBRICANT ANALYSIS

The elemental analysis of fuels showed that RME has 10.6% mass oxygen content, whereas diesel has only 0.2% mass oxygen content. Total nitrogen of RME is 7.8 mg/kg and of diesel is 2.2 mg/kg. Together with the higher combustion temperature of RME when EGR is not used, these results can explain the higher levels of NOx emissions with RME than with diesel.

The most notable result of the engine lubricant analysis was that Fe concentration of the used oil (6 wt. ppm) was higher than that of the new oil (1 wt. ppm). If engine wear metals and corrosion particles were seen on TEM grids, they would exist as separate particles not bound to any carbonaceous PM [48]. This not being the case indicates that wear metals of the engine were collected by the lubricant instead of being emitted in the exhaust.

PM originating from engine wear was previously found to be in much lower quantity than PM originating from the engine lubrication oil [48]. Soot (accumulation mode) acts as a very efficient sink for nucleation mode particles to coagulate on. In the absence of a soot mode, the particles will grow by coagulation (between the smaller particles) and condensational growth and are therefore not scavenged [49]. The large amount of nanoparticles, i.e. the nucleation mode, when the engine was operating without EGR were visible because there was no soot. It is thought that they are lubrication-derived particles, as previously shown in [40][41].

SUMMARY AND CONCLUSIONS

By increasing EGR levels from 0 at 20.95% intake O_2 concentration to approximately 60% at very low intake O_2 concentration of ~8%, different low load operation conditions of a single cylinder Scania D13 HD engine were achieved while using three fuels: petroleum-based diesel, RME and their mixture B20. This strategy was employed in order to produce emissions of PM with a range of different properties, which were then studied in order to understand particulate mass emissions of the total black carbon (BC) and organic aerosol (OA), particle size distributions and the soot nanostructure by means of transmission electron microscopy (TEM). Additionally, regulated gaseous emissions were analysed.

The key conclusions of this study are:

- Due to the soot reduction factors of RME ranging from ~2 (for low EGR) to ~3-4 (for high EGR) compared to diesel, RME gives a possibility to utilise higher levels of EGR and stay in the region of low NOx, CO and THC emissions, while producing less soot than with diesel and B20.

- The organic fraction of the PM was dominant at low-sooting conditions with no EGR. For this case, unregulated nanoparticles of size between 5 nm and 23 nm, which are thought to originate from the lubrication oil, were emitted in high numbers as nucleation mode.

- Accumulation mode particles had mean diameter from 44-55 nm at low EGR to 125-160 nm at high EGR levels. At all comparable EGR levels, RME had lowest indicated specific total TPNC, followed by B20 and diesel. The gain of using RME is most significant at EGR rate of 44% for the engine operating conditions regarded in this study.

- RME and diesel branched soot agglomerates were composed of several tens to hundreds of primary particles 20-30 nm in diameter and lattice distances of 0.35-0.4 nm. B20 soot agglomerates were of similar shape and size, but the primary particles, however, seem to be “melted” together and often indistinguishable. In addition to the regular soot particles, diesel soot contained fly ashes possibly originating from the combusted engine lubrication oil.

This study was done as a continuation of the previous work with exhaust analysis for diesel and light alcohols in the same type of a HD CI experimental engine [41]. A new area for further research can be an extension of this study to other biofuels, for example to hydrotreated vegetable oil (HVO) as in [50], and further studies of the effect of varying EGR levels on particle emissions, for example emissions of polycyclic aromatic hydrocarbons (PAHs) and other black carbon precursors. An exhaust aftertreatment system can also be included in order to determine the

effects it can have on the physical and chemical properties of PM, as well as on the regulated emissions.

ACKNOWLEDGMENTS

The authors would like to acknowledge the KCFP Engine Research Center, Swedish Energy Agency (grant number 22485-4), the Swedish research councils FORMAS (2016-00697), VR (2018-04200) and AFA insurance (160323) for their support and financing. A sincere thank you to Yann Gallo and Mengqin Shen for their technical assistance.

REFERENCES

1. Forster, P., Ramaswamy, V., Artaxo, P., Berntsen, T. et al., "Changes in Atmospheric Constituents and in Radiative Forcing," in *Climate Change 2007: The Physical Science Basis. Contribution of Working Group I to the Fourth Assessment Report of the Intergovernmental Panel on Climate Change*, Solomon, S., Qin D., Manning M., Chen Z. et al. Eds., Cambridge, United Kingdom and New York, NY, USA, Cambridge University Press, 2007, 129-234.
2. U.S. EPA, "Inventory of U.S. Greenhouse Gas Emissions and Sinks: 1990–2014," U.S. EPA Office of Air and Radiation, EPA 430-R-16-002, 2016.
3. IPCC, Edenhofer, O., Pichs-Madruga, R., Sokona, Y., Farahani, E. et al. Eds., "Climate Change 2014: Mitigation of Climate Change. Contribution of Working Group III to the Fifth Assessment Report of the Intergovernmental Panel on Climate Change," Cambridge, United Kingdom and New York, NY, USA, Cambridge University Press, 2014.
4. U.S. EPA. "Inventory of U.S. Greenhouse Gas Emissions and Sinks: 1990–2016," EPA 430-R-18-003, 2018.
5. EEA, "Annual European Union Greenhouse Gas Inventory 1990-2016 and Inventory Report 2018," EEA Report No 5, 2018.
6. Bond, T. C., Doherty, S. J., Fahey, D. W., Forster, P. M. et al., "Bounding the Role of Black Carbon in the Climate System: A Scientific Assessment," *J. Geophys. Res. Atmos.* 118:5380-5552, 2013, doi:10.1002/jgrd.50171.
7. Ramanathan, V., and Carmichael, G., "Global and Regional Climate Changes due to Black Carbon," *Nature Geosci.* 1(4):221-227, 2008, doi:10.1038/ngeo156.
8. IPCC, Stocker, T.F., Qin, D., Plattner, G. K., Tignor, M. et al. Eds., "Climate Change 2013: The Physical Science Basis, Contribution of Working Group I to the Fifth Assessment Report of the Intergovernmental Panel on Climate Change," Cambridge, United Kingdom and New York, NY, USA, Cambridge University Press, 2013, doi:10.1017/CBO9781107415324.
9. Jimenez, J. L., Canagaratna, M. R., Donahue, N. M., Prevot, A. S. H. et al. "Evolution of Organic Aerosols in the Atmosphere," *Science* 326:1525-1529, 2009, doi:10.1126/science.1180353.
10. Zhang, Q., Jimenez, J. L., Canagaratna, M. R., Allan, J. D. et al., "Ubiquity and Dominance of Oxygenated Species in Organic Aerosols in Anthropogenically-Influenced Northern Hemisphere Midlatitudes," *Geophys. Res. Lett*. 34, L13801, doi:10.1029/2007GL029979.
11. Zhu Q., Huang X. F., Cao L. M., Wei L. T. et al., "Improved Source Apportionment of Organic Aerosols in Complex Urban Air Pollution Using the Multilinear Engine (ME-2)," *Atmos. Meas. Tech.* 11:1049-1060, 2018, doi:10.5194/amt-11-1049-2018.
12. Hallquist, M., Wenger, J. C., Baltensperger, U., Rudich, Y. et al., "The Formation, Properties and Impact of Secondary Organic Aerosol: Current and Emerging Issues," *Atmos. Chem. Phys.* 9:5155-5236, 2009, doi:10.5194/acp9-5155-2009.
13. Borm, P. J., Schins, R. P., and Albrecht, C., "Inhaled Particles and Lung Cancer, Part B: Paradigms and Risk Assessment," *Int. J. Cancer* 110(1):3-14, 2004, doi:10.1002/ijc.20064.
14. Ostiguy, C., Soucy, B., Lapointe, G., Woods, C. et al., "Health Effects of Nanoparticles, Second Edition," IRSST Report R-589, 2006.
15. European Commission, "Commission Regulation (EC) No 692/2008 of 18 July 2008 Implementing and Amending Regulation (EC) No. 715/2007 of the European Parliament and of the Council on Type Approval of Motor Vehicles with Respect to Emissions from Light Passenger and Commercial Vehicles (Euro 5 and Euro 6) and on Access to Vehicle Repair and Maintenance Information," *Off. J. Eur. Union* L199:1–136, 2008.
16. European Commission, "Commission Regulation (EU) No 582/2011 of 25 May 2011 Implementing and Amending Regulation (EC) No 595/2009 of the European Parliament and of the Council with Respect to Emissions from Heavy-Duty Vehicles (Euro VI) and Amending Annexes I and III to Directive 2007/46/EC of the European Parliament and of the Council," *Off. J. Eur. Union* L167:1–168, 2011.
17. Giechaskiel, B., "Solid Particle Number Emission Factors of Euro VI Heavy-Duty Vehicles on the Road and in the Laboratory," *Int. J. Environ. Res. Public Health* 15(2):304, 2018, doi:10.3390/ijerph15020304.
18. Vander Wal, R. L., and Tomasek, A. J., "Soot Oxidation: Dependence upon Initial Nanostructure," *Combustion and Flame* 134(1-2):1-9, 2003, doi:10.1016/S0010-2180(03)00084-1.
19. Boehman, A. L., Song J. and Alam M., "Impact of Biodiesel Blending on Diesel Soot and the Regeneration of Particulate Filters," *Energy Fuels* 19:1857-1864, 2005, doi:10.1021/ef0500585.
20. Malmborg, V. B., Eriksson, A. C., Shen, M., Nilsson, P. et al., "Evolution of In-Cylinder Diesel Engine Soot and Emission Characteristics Investigated with Online Aerosol Mass Spectrometry," *Environ. Sci.*

Technol. 51(3):1876-1885, 2017, doi:10.1021/acs.est.6b03391.
21. Horn, U., Egnell, R., Johansson, B., and Andersson, O., "Detailed Heat Release Analyses with Regard to Combustion of RME and Oxygenated Fuels in an HSDI Diesel Engine," SAE Technical Paper 2007-01-0627, 2007, doi:10.4271/2007-01-0627.
22. Lapuerta, M., Armas, O. and Rodriguez-Fernandez, J., "Effect of Biodiesel Fuels on Diesel Engine Emissions," *Prog. Energy Combust. Sci.* 34(2):198−223, 2008, doi:10.1016/j.pecs.2007.07.001.
23. Mende, T., Ando, R., Nagata, M., Kato, H. et al., "Detailed Analysis of Particulate Matter Emitted from Biofueled Diesel Combustion with High EGR," SAE Technical Paper 2009-01-0483, 2009, doi:10.4271/2009-01-0483.
24. Aoyagi, Y., Shimada, K., Osada, H., Noda, A. et al., "Diesel Emissions Improvement by RME in a High Boost and EGR Single Cylinder Engine," SAE Technical Paper 2008-01-1376, 2008, doi:10.4271/2008-01-1376.
25. Savic, N., Rahman, M., Miljevic, B., Saathoff, H. et al., "Influence of Biodiesel Fuel Composition on the Morphology and Microstructure of Particles Emitted from Diesel Engines," *Carbon* 104:179-189, 2016, doi:10.1016/j.carbon.2016.03.061.
26. Ban-Weiss, G. A., Chen, J. Y., Buchholz, B. A., and Dibble, R. W., "A Numerical Investigation into the Anomalous Slight NOx Increase When Burning Biodiesel; A New (Old) Theory," *Fuel Process. Technol.* 88(7):659-667, 2007, doi:10.1016/j.fuproc.2007.01.007.
27. Cheng, A. S., Upatnieks, A., and Mueller, C. J., "Investigation of the Impact of Biodiesel Fuelling on NOx Emissions Using an Optical Direct Injection Diesel Engine", *Int. J. Engine Res.* 7:297-318, 2006, doi:10.1243/14680874JER05005.
28. Li, C., Yin, L., Shamun, S., Tuner, M. et al., "Transition from HCCI to PPC: The Sensitivity of Combustion Phasing to the Intake Temperature and the Injection Timing with and without EGR," SAE Technical Paper 2016-01-0767, 2016, doi:10.4271/2016-01-0767.
29. Schindler, W., Haisch, C., Beck, H., Niessner, R. et al., "A Photoacoustic Sensor System for Time Resolved Quantification of Diesel Soot Emissions," SAE Technical Paper 2004-01-0968, 2004, doi:10.4271/2004-01-0968.
30. Cambustion Limited, "Fast Response Aerosol Size Measurements with the DMS500," cambustion.com/products/dms500/aerosol, accessed Aug. 2018.
31. Onasch, T. B., Trimborn, A., Fortner, E. C., Jayne, J. et al., "Soot Particle Aerosol Mass Spectrometer: Development, Validation, and Initial Application," *Aerosol Sci. Technol.* 46(7):804-817, 2012, doi:10.1080/02786826.2012.663948.
32. DigitalMicrograph Computer Software, Gatan Inc., Pleasanton, VA, USA, 2017.
33. Lieke, K. I., Rosenorn, T., Pedersen, J., Larsson, D. et al., "Micro- and Nanostructural Characteristics of Particles Before and After an Exhaust Gas Recirculation System Scrubber," *Aerosol Sci. Technol.* 47(9):1038-1046, 2013, doi:10.1080/02786826.2013.813012.
34. Vander Wal, R. L., Bryg, V. M. and Hays, M. D., "Fingerprinting Soot (Towards Source Identification): Physical Structure and Chemical Composition," *J. Aerosol Sci.* 41(1):108-117, 2010, doi:10.1016/j.jaerosci.2009.08.008.
35. Yehliu, K., Vander Wal, R. L. and Boehman, A. L., "Development of an HRTEM Image Analysis Method to Quantify Carbon Nanostructure," *Combust. Flame* 158:1837-1851, 2011, doi:10.1016/j.combustflame.2011.01.009.
36. Schneider, C. A., Rasband, W. S., and Eliceiri, K. W., "NIH Image to ImageJ: 25 years of image analysis," *Nature Methods* 9(7):671-675, 2012, PMID:22930834.
37. Hoekman, S. and Robbins, C., "Review of the effects of biodiesel on NOx emissions," *Fuel Process. Technol.* 96:237-249, 2012, doi:10.1016/j.fuproc.2011.12.036.
38. Mancaruso, E., Vaglieco, B., and Ciaravino, C., "Combustion Analysis in an Optical Diesel Engine Operating with Low Compression Ratio and Biodiesel Fuels," SAE Technical Paper 2010-01-0865, 2010, doi:10.4271/2010-01-0865.
39. Graboski, M. S and McCormick, R. L., "Combustion of fat and vegetable oil derived fuels in diesel engines," *Prog. Ener. Combust.* 24(2):125-164, 1998, doi:10.1016/S0360-1285(97)00034-8.
40. Canagaratna, M. R., Jayne, J. T., Ghertner, D. A., Herndon, S. et al., "Chase Studies of Particulate Emissions from in-use New York City Vehicles," *Aerosol Sci. Technol.* 38(6):555-573, 2004, doi:10.1080/02786820490465504.
41. Shamun, S., Novakovic, M., Malmborg, V. B., Preger, C. et al., "Detailed Characterization of Particulate Matter in Alcohol Exhaust Emissions," Presented at COMODIA 2017, Japan, July 25-28, 2017, doi:10.1299/jmsesdm.2017.9.B304.
42. Hinds, W. C., "Aerosol Technology: Properties, Behaviour, and Measurement of Airborne Particles, Second Edition," (New York, John Wiley & Sons, 1999), ISBN: 978-0-471-19410-1.
43. Zhu, L., Cheung, C. S., Zhang, W. G. and Huang, Z., "Influence of Methanol–Biodiesel Blends on the Particulate Emissions of a Direct Injection Diesel Engine," *Aerosol Sci. Technol.* 44(5):362-369, 2010, doi:10.1080/02786821003652646.
44. Obelin, A., "High Resolution TEM Studies of Carbonization and Graphitization," *Chem. Phys. Carbon* 22, Thrower, P. A. Ed., New York, NY, USA, Marcel Dekker, 1989, 1-143.
45. Pawlyta, M., Rouzaud, J. N., and Duber, S., "Raman Microspectroscopy Characterization of Carbon Blacks. Spectral Analysis and Structural Information," *Carbon* 84:479-490, 2015, doi:10.1016/j.carbon.2014.12.030.
46. Torok, S., Malmborg, V. B., Simonsson, J., Eriksson, A. et al., "Investigation of the Absorption

Angstrom Exponent and Its Relation to Physicochemical Properties for Mini-CAST Soot," *Aerosol Sci. Technol.* 52(7):757-767, 2018, doi:10.1080/02786826.2018.1457767.
47. Malmborg, V. B., Eriksson, A. C., Torok, S., Zhang, Y. et al., "Relating Aerosol Mass Spectra to Composition and Nanostructure of Soot Particles," *Carbon*, 2018, doi:10.1016/j.carbon.2018.10.072.
48. Sappok, A. and Wong, V., "Detailed Chemical and Physical Characterization of Ash Species in Diesel Exhaust Entering Aftertreatment Systems," SAE Technical Paper 2007-01-0318, 2007, doi:10.4271/2007-01-0318.
49. Wang, H., "Formation of Nascent Soot and Other Condensed-Phase Materials in Flames," *Proc. Combust. Inst.* 33:41–67, 2011, doi:10.1016/j.proci.2010.09.009.
50. Shukla, P., Shamun, S., Gren, L., Malmborg, V. et al., "Investigation of Particle Number Emission Characteristics in a Heavy-Duty Compression Ignition Engine Fueled with Hydrotreated Vegetable Oil (HVO)," SAE Technical Paper 2018-01-0909, 2018, doi:10.4271/2018-01-0909.
51. Blackenfelt, P., Perstorp Holding AB, personal communication, Sept. 2018.

CONTACT

Maja Novakovic
PhD Candidate
Division of Combustion Engines
Department of Energy Sciences
Lund University, Sweden
Maja.Novakovic@energy.lth.se

DEFINITIONS AND ABBREVIATIONS

BC: black carbon

CA50: The crank angle at which 50% of the charge has been consumed.

CAD ATDC: crank angle degrees after top dead centre

CAD BTDC: crank angle degrees before top dead centre

CDC: conventional diesel combustion

CI: compression ignition

CLD: chemiluminescence detector

CMD: count mean diameter

CN: cetane number

DEP: diesel exhaust particles

DMS: differential mobility spectrometer

DOC: diesel oxidation catalyst

DPF: diesel particulate filter

eBC: equivalent black carbon

EDS: energy-dispersive spectrometer

EGR: exhaust gas recirculation

FAME: fatty acid methyl ester

FID: flame ionization detector

GHG: greenhouse gas

GSD: geometrical standard deviation

HD: heavy duty

HVO: hydrotreated vegetable oil

ICE: internal combustion engine

$IMEP_G$: gross indicated mean effective pressure

IRD: infrared detector

MSS: micro-soot sensor

NOx: nitrogen oxides

OA: organic aerosol

PAH: polycyclic aromatic hydrocarbons

PM: particulate matter

PMD: paramagnetic detector

PMP: particle measurement program

Q_{LVH}: lower heating value

rBC: refractory black carbon

RME: rapeseed oil methyl esters

RoHR: rate of heat release

SCR: selective catalytic reduction

SOI: start of injection

SP-AMS: soot-particle aerosol mass spectrometer

SPN: solid particle number

TEM: transmission electron microscope

THC: total hydrocarbons

TPNC: total particulate number concentration

UFP: ultrafine particle

VOC: volatile organic compound

λ: Lambda, the ratio between the air-fuel ratio and the stoichiometric air-fuel ratio for the given fuel, $\left(\frac{A}{F}\right)/\left(\frac{A}{F}\right)_S$.

APPENDIX A: FUELS

Table A-1. Fuels nomenclature.

Common acronym	In the paper text	Fuel description
B0	diesel	Swedish MK-1 petroleum-based diesel
B20	B20	blend: 20 volume-% B100 and 80 volume-% B0
B100	RME	rapeseed oil methyl esters biodiesel

Table A-2. Chemical composition of RME (B100) fuel [51].

Generic chemical description	IUPAC name (dossier)	EC no	CAS no	Typical conc. (%)
C16 Methyl ester, saturated	Methyl Hexadecanoate	203-966-3	112-39-0	5
C16 Methyl ester, unsaturated (mono)	methyl (Z)-hexadec-9-enoate	214-303-2	1120-25-8	0,2
C18 Methyl ester, saturated	Methyl Octadecanoate	203-990-4	112-61-8	1,7
C18 Methyl ester, unsaturated (mono)	Methyl (Z)-octadec-9-enoate	203-992-5	112-62-9	60
C18 Methyl ester, unsaturated (di)	methyl (9Z,12Z)-octadeca-9,12-dienoate	203-993-0	112-63-0	20
C18 Methyl ester, unsaturated (tri)	methyl (9Z,12Z,15Z)-octadeca-9,12,15-trienoate	206-102-3	301-00-8	9,5
C20 Methyl ester, saturated	Methyl icosanoate	214-304-8	1120-28-1	0,5
C20 Methyl ester, unsaturated (mono)	11-Eicosenoic acid methyl ester		3946-08-05	1,2
C22 Methyl ester, saturated	methyl docosanoate	213-207-8	929-77-1	0,3
C22 Methyl ester, unsaturated (mono)	methyl (Z)-docos-13-enoate	214-305-3	1120-34-9	0,3
C24 Methyl ester, saturated	methyl tetracosanoate	219-475-2	2442-49-1	0,1
C24 Methyl ester, unsaturated (mono)	15-Tetracosenoic acid methyl ester		56544-33-7	0,2

APPENDIX B: AEROSOL SIZE DISTRIBUTION PARAMETERS

Table B-1. Particle CMD, GSD and TPNC for nucleation mode and accumulation mode particles in exhaust of for diesel, RME and B20 combustion.

O_2 [%]	CMD [nm]		GSD [-]		TPNC [#/cm^3]		
	nuc. mode	acc. mode	nuc. mode	acc. mode	nuc. mode	acc. mode	total
diesel							
20.9	26.1±3.92	54.73±39.63	1.35±0.14	1.62±0.20	1.76x10^6±1.08x10^6	9.68x10^5±6.1x10^5	3.0x10^6±5.37x10^5
15.2	20.59±9.60	105.88±2.79	1.35±0.12	1.69±0.03	1.63x10^3±1.6x10^4	5.15x10^5±8.25x10^4	9.14x10^5±1.55x10^5
13.3	27.50±0.0014	150.25±1.63	1.45±0.02	1.48±0.01	4.08x10^3±3.12x10^4	1.27x10^6±1.38x10^5	2.54x10^6±2.82x10^5
11.4	26.61±0.95	156.20±1.38	1.55±0.05	1.55±0.01	0±0	1.64x10^6±4.91x10^4	3.28x10^6±1.35x10^5
11.3	27.50±0.008	150.10±1.10	1.54±0.06	1.50±0.009	8.59x10^4±5.05x10^4	2.54x10^6±6.8x10^4	4.98x10^6±1.35x10^5
8.5	22.50±4.53	115.20±5.36	1.43±0.13	1.52±0.07	1.08x10^4±6.1x10^4	5.4x10^5±3.19x10^5	9.55x10^5±5.57x10^5
RME							
20.9	27.25±1.14	36.40±4.61	1.33±0.03	1.53±0.06	1.23x10^6±5.27x10^5	6.33x10^5±3.37x10^5	1.99x10^6±2.25x10^5
14.9	9.03±1.78	99.81±3.28	1.12±0.04	1.61±0.03	4.67x10^2±5.76x10^3	1.57x10^5±1.16x10^4	2.72x10^5±2.64x10^4
13.6	14.94±0	128.54±10.44	1.18±0	1.72±0.21	0±0	6.59x10^4±6.54x10^3	1.26x10^5±1.51x10^4
12.4	8.30±1.27	127.89±2.25	1.11±0.003	1.42±0.02	0±0	6.2x10^5±9.7x10^4	1.13x10^6±1.83x10^5
11.7	9.65±1.90	129.14±1.75	1.11±0.003	1.40±0.009	2.14x10^2±4.95x10^3	7.72x10^5±7.28x10^4	1.42x10^6±1.41x10^5
9.4	12.07±0.12	124.43±6.55	1.11±0	1.48±0.02	0±0	5.56x10^5±4.52x10^4	9.91x10^5±1.03x10^5
B20							
20.9	25.34±4.54	43.91±21.20	1.33±0.11	1.47±0.12	8.84x10^5±6.67x10^5	9.28x10^5±5.07x10^5	2.10x10^6±3.35x10^5
15.4	27.33±1.12	96.37±2.36	1.21±0.18	1.76±0.02	2.24x10^4±1.07x10^4	2.1x10^5±1.01x10^4	3.64x10^5±2.14x10^4
13.3	11.69±0.27	147.85±1.46	1.12±0.03	1.43±0.02	6.42x10^3±4.03x10^4	1.07x10^6±8.18x10^4	2.16x10^6±1.73x10^5
10.7	12.04±1.26	163.37±2.01	1.12±0.02	1.51±0.01	1.97x10^4±8.43x10^4	2.13x10^6±3.82x10^4	4.46x10^6±1.31x10^5
8.9	12.04±1.26	167.09±17.96	1.15±0.09	1.74±0.06	99±1.1x10^3	2.56x10^4±1.47x10^4	5.56x10^4±3.34x10^4

APPENDIX C: TEM IMAGES

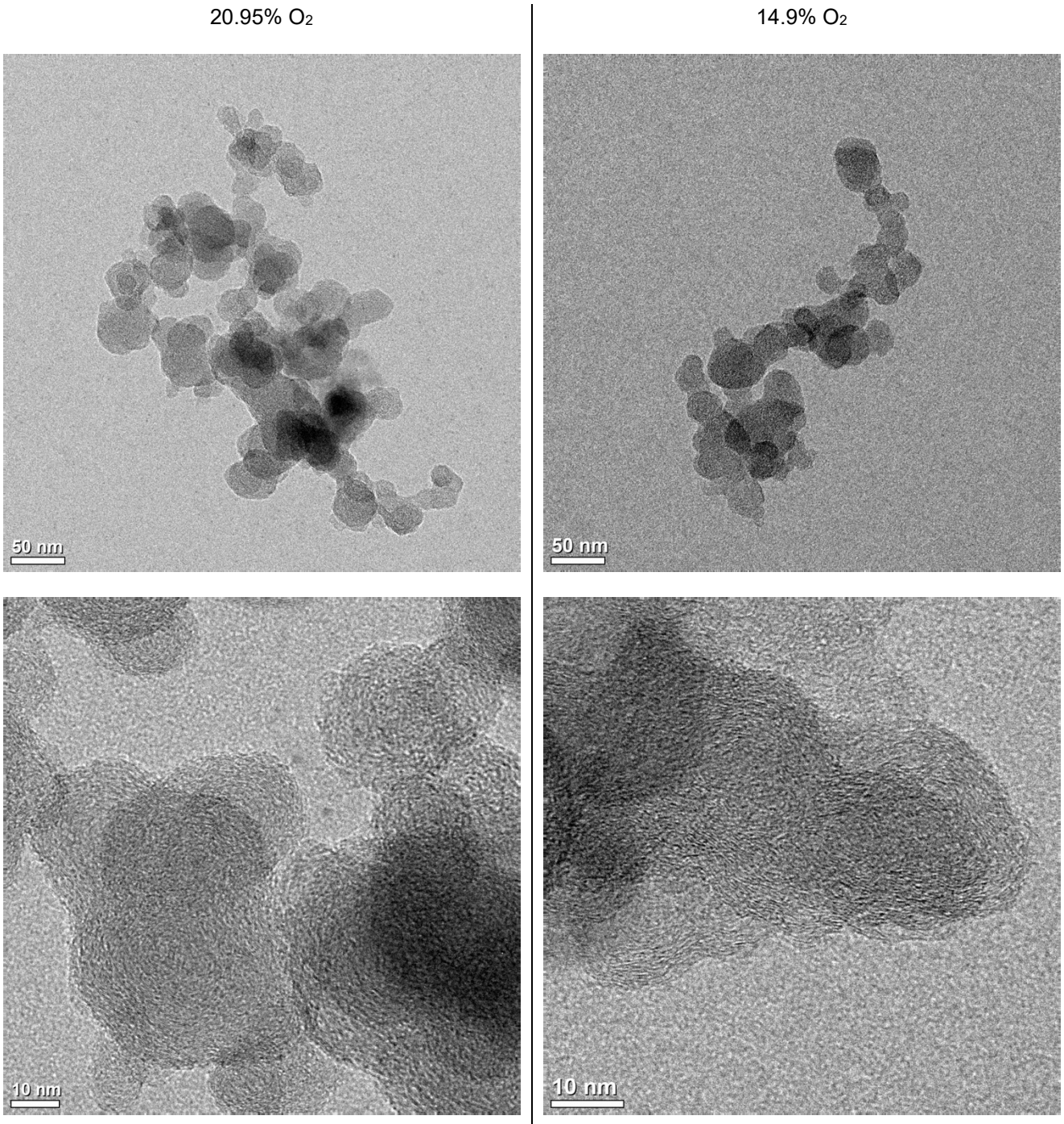

Figure C-1. TEM images of soot nanostructure for RME at two intake O_2 concentration levels: left 20.95% and right 14.9%. Size scale: top row 50 nm (overview) and bottom row 10 nm (high resolution). Fuels nomenclature given in Table A-1 in Appendix A.

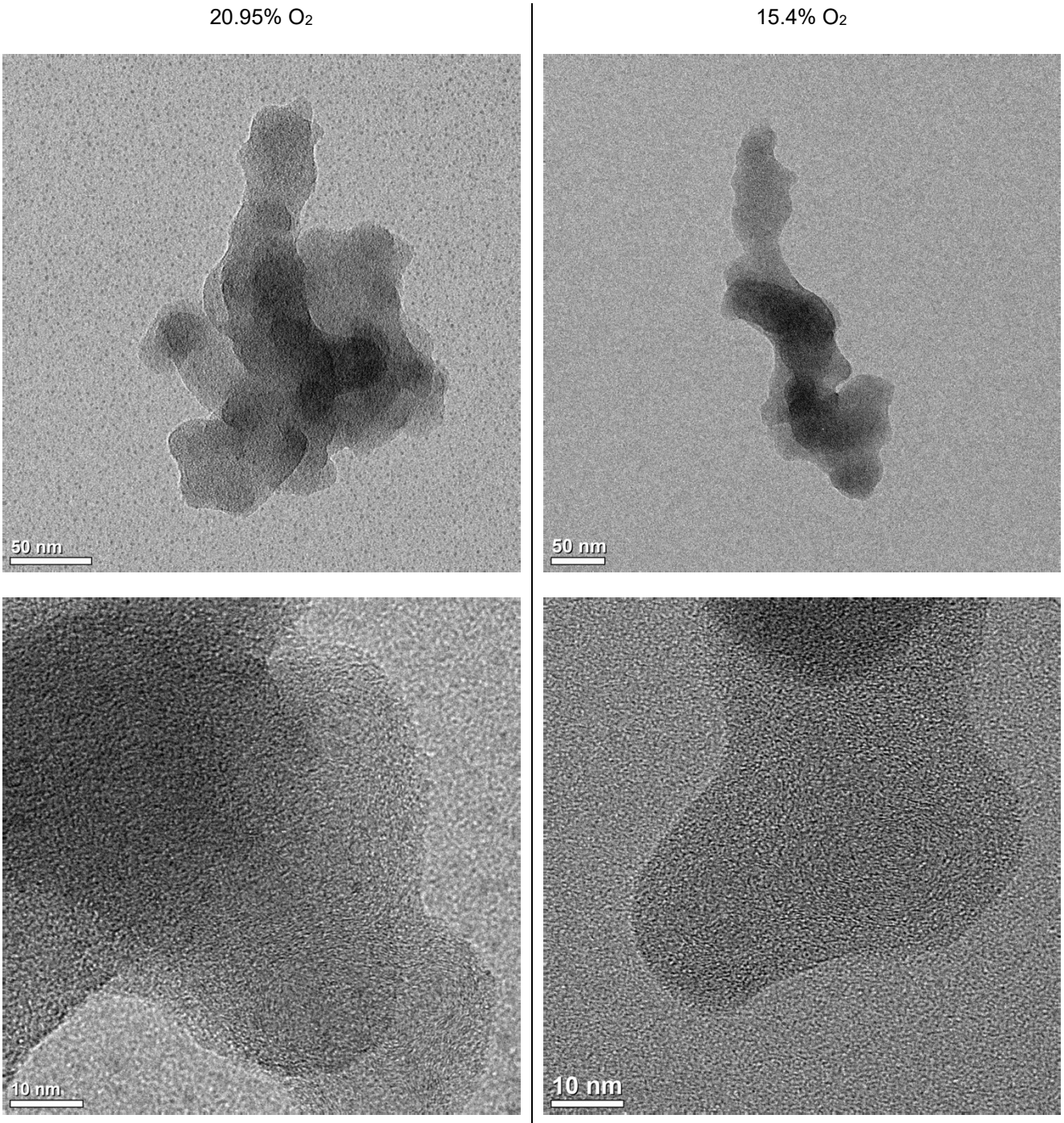

Figure C-2. TEM images of soot nanostructure for B20 at two intake O_2 concentration levels: left 20.95% and right 15.4%. Size scale: top row 50 nm (overview) and bottom row 10 nm (high resolution). Fuels nomenclature given in Table A-1 in Appendix A.

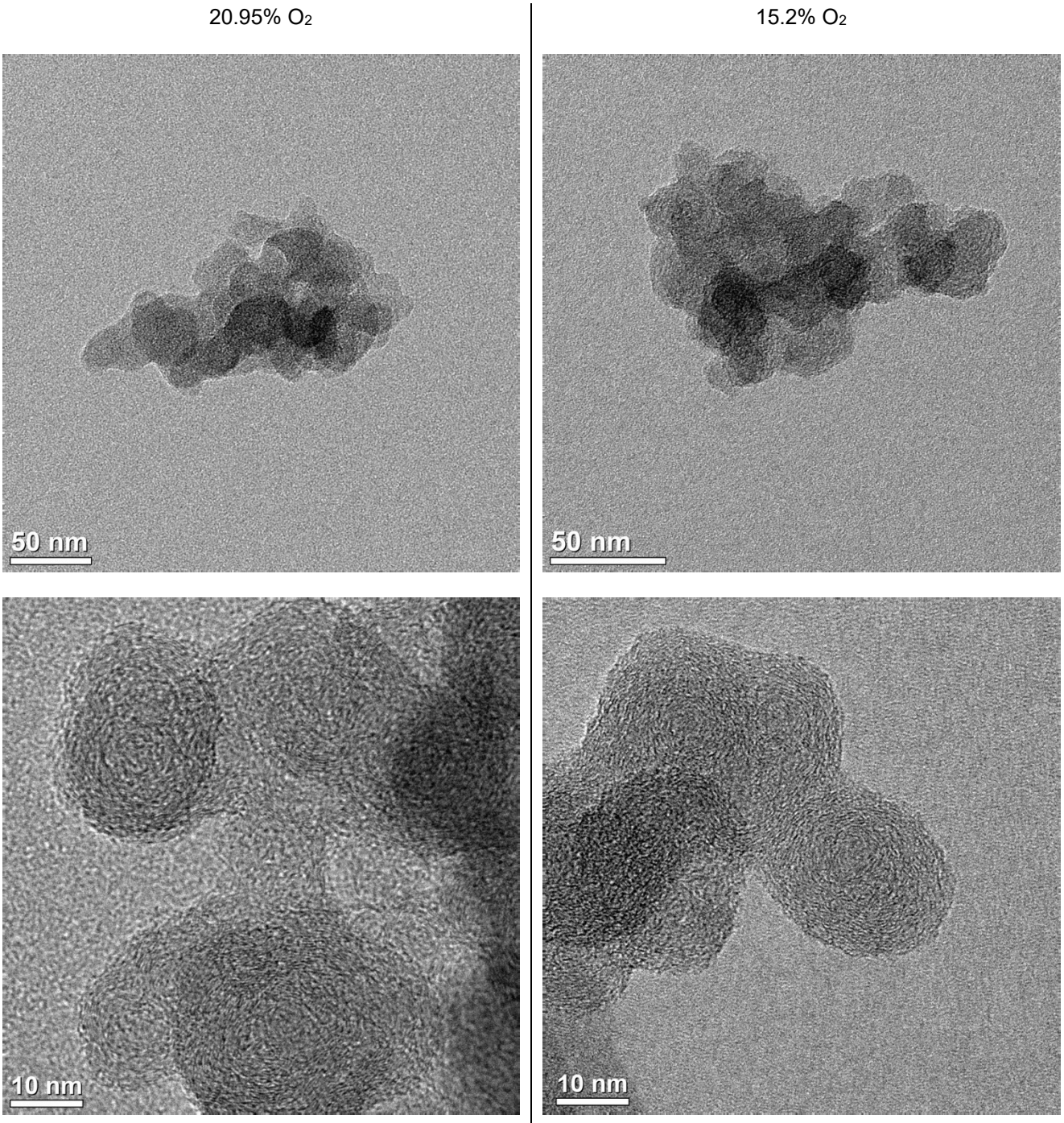

Figure C-3. TEM images of soot nanostructure for diesel at two intake O_2 concentration levels: left 20.95% and right 15.2%. Size scale: top row 50 nm (overview) and bottom row 10 nm (high resolution). Fuels nomenclature given in Table A-1 in Appendix A.